A&A 532, A154 (2011)
DOI: 10.1051/0004-6361/201116667


Astronomy & Astrophysics

# VLT optical *BVR* observations of two bright supernova Ia hosts in the Virgo cluster

## Surface brightness fluctuation analysis

M. Cantiello[1], I. Biscardi[1,2], E. Brocato[1], and G. Raimondo[1]

[1] INAF – Osservatorio Astronomico di Teramo, via M. Maggini snc, 64100 Teramo, Italy
e-mail: cantiello@oa-teramo.inaf.it
[2] Dipartimento di Fisica – Universitá di Roma Tor Vergata, via della Ricerca Scientifica 1, 00133 Rome, Italy

Received 7 February 2011 / Accepted 6 June 2011

**ABSTRACT**

*Aims.* We study the characteristics of field stars in the two bright ellipticals NGC 4621 and NGC 4374 in the Virgo cluster to derive accurate distances and stellar population properties. Moreover, since the target galaxies have hosted three type Ia supernova events, we investigate the possible correlations between the SNe Ia properties and their host stellar systems.
*Methods.* Using deep imaging *BVR* data, obtained with the FORS2 camera mounted at the VLT, we analysed the surface brightness fluctuations (SBF) properties of the targets. We adopted our measurements and existing empirical or theoretical calibrations to estimate the distance of the NGC 4621 and NGC 4374. For stellar population analysis, we measured SBF amplitudes in different galaxy regions, allowing us to study the changes in field star properties. The three-band coverage of present data, coupled with existing SBF measures available from the literature, provides us with the broadest wavelength coverage of SBF magnitudes for single objects. We present a detailed comparison between SBF data and models to constrain the physical characteristics of the dominant stellar components at i) various galactic radii; and ii) in the regions where SNe Ia events were recorded.
*Results.* Our *V* and *R* SBF measures, coupled with either empirical or theoretical calibrations, provide distance moduli in agreement with literature estimates. The median of our and literature SBF-based distances agrees with the median obtained from non-SBF methods, indicating the absence of any systematic effect in the SBF technique. The same result holds for SBF and SN Ia distances. Comparing either the SBF versus integrated colour diagrams, or the SBF versus SBF colour diagrams, with SPoT models, we find that stellar population properties do not change significantly along the galactic radius, with a dominant population having old age and nearly solar chemical composition. The galaxies appear similar in all properties analysed, except for *B*-band SBF. Since the SBF magnitudes in this band are sensitive to the properties of the hot stellar component, we speculate that such behaviour can be a consequence of different diffuse hot stellar components in the two objects. By using specific models, we find that the presence of a percentage of hot HB stars in old and metal-rich stellar population could be at the origin of the observed differences. Finally, we find a good uniformity in the *V* and *R* SBF and integrated colours in the regions where the three SNe Ia, presenting different absolute luminosities, exploded. On the other hand, the SBF signal measured in the *B*-band shows intriguing differences.

**Key words.** galaxies: elliptical and lenticular, cD – galaxies: stellar content – galaxies: clusters: individual: NGC 4621 – galaxies: clusters: individual: NGC 4374 – galaxies: photometry – galaxies: distances and redshifts

## 1. Introduction

Our understanding of galaxies in the distant Universe relies on how well we understand the properties of their local templates. Thus, the study of nearby unresolved stellar populations plays a key role in obtaining a refined characterisation of stellar populations at higher redshifts. Although different astronomical methods exist to carry out such detailed analysis, none of them can provide robust constraints by itself. The presence of internal uncertainties in each method, or calibration uncertainties, as well as the effect of the age-metallicity degeneracy that affects most of the spectro-photometric indicators (Worthey 1994), prevents us from relying on one single stellar population tracer for these studies, and pushes the community of astronomers towards defining new analysis methods.

In the past two decades, the SBF method, introduced by Tonry & Schneider (1988) to obtain distances of early-type galaxies, has proved itself not only an accurate and precise distance indicator, but also a powerful tracer of stellar population properties (e.g., Jensen et al. 2003; Raimondo et al. 2005; Cantiello et al. 2007b). By definition, the SBF magnitude corresponds to the ratio of the second to the first moment of the stellar luminosity function in the galaxy: $\bar{m} = -2.5 \log \bar{f}$, where $\bar{f} \equiv \frac{\Sigma_i n_i f_i^2}{\Sigma_i n_i f_i}$, and $n_i$ is the number of stars per bin of flux $f_i$ (Tonry & Schneider 1988). Such definition implies that (i) SBF magnitudes are linked to the properties of the stars in the galaxy; (ii) the SBF signal is dominated by the brightest stellar component in the galaxy, because of the dependence on the second moment of the luminosity function; (iii) since the brightest phase in a stellar population is wavelength-dependent, SBF magnitudes in different pass-bands are sensitive to the properties of stars in different, well-defined evolutionary stages (Worthey 1993a; Brocato et al. 1998; Cantiello et al. 2003).

Taking advantage of archival *B*, *V*, and *R* observations taken with the FORS2 camera of the Very Large Telescope for two

**Table 1.** Main parameters of the target galaxies and observations.

| | NGC 4621 | NGC 4374 |
|---|---|---|
| | Galaxy parameters | |
| RA(J2000)[1] | $12^h42^m02.3^s$ | $12^h25^m03.7^s$ |
| Dec(J2000)[1] | $+11^d38^m49^s$ | $+12^d53^m13^s$ |
| Galaxy Type[2] | E5 | E |
| Morphological T-Type[2] | –4.8 | –4.3 |
| Absolute $B$-band magnitude[2] | –20.5 | –21.0 |
| SNe Ia events | SN1939B | SN1957B, SN1991bg |
| $cz$[1] (km s$^{-1}$, Heliocentric) | $410 \pm 6$ | $1060 \pm 6$ |
| $E(B-V)$[3] | 0.033 mag | 0.040 mag |
| $(V-I)$[4] | $1.172 \pm 0.018$ | $1.191 \pm 0.008$ |
| | Observations | |
| Filter | Exposure time (s) | Exposure time (s) |
| $B$ | 3375 | 2250 |
| $V$ | 3375 | 2250 |
| $R$ | 2376 | 1584 |

**Notes.** [(1)] Data retrieved from NED (http://nedwww.ipac.caltech.edu). [(2)] Hyperleda (http://leda.univ-lyon1.fr). [(3)] Schlegel et al. (1998). [(4)] Tonry et al. (2001).

bright early-type galaxies in the Virgo cluster, NGC 4621 and NGC 4374, we obtain multi-band SBF measurements of these galaxies. These measurements, coupled with existing ground-based $I$- and $K$-band measures and space-based $F850LP$ from ACS data ($z$ hereafter; for integrated colours we also use ACS $F475W$ data, indicated as $g$ in the paper), provide the broadest wavelength coverage of SBF measures for single galaxies. With this sample of measurements, we investigate the properties of the two galaxies using the SBF technique under its twofold aspects: as a distance indicator and as a tracer of stellar population properties. Furthermore, since the target galaxies have hosted three SNe Ia events – SN 1939B in NGC 4621 (Zwicky 1942), SN 1957B (Bertola 1964, and references therein), and SN 1991bg (Kosai et al. 1991) in NGC 4374 – we can explore the capabilities of the SBF method to improve our knowledge on the relation between the SNe Ia progenitors and the stellar population they belong to.

The paper is organised as follow. A description of the observational data set, the data reduction and calibration procedures, and the procedure for SBF measurements is given in Sect. 2. The analysis of distances is presented in Sect. 3, while the study of stellar population properties based on SBF is presented in Sect. 4. A summary and the conclusions finish the paper in Sect. 5.

## 2. The data

For this work we used $B$, $V$, and $R$ data of two Virgo cluster galaxies, NGC 4621 and NGC 4374, observed with the FORS2 camera of the VLT. Some relevant properties of the targets are reported in Table 1. The science images of the galaxies and the calibration files (bias, flat, field of standard stars) were retrieved from the ESO archive[1]. In one case, NGC 4374, we could not use the total integration time available because of a slight rotation ($\lesssim$1 deg) between different frames which badly affects the SBF signal (see below). In Table 1 we list the total exposure times for each filter and for both galaxies.

[1] http://archive.eso.org/

### 2.1. Data reduction and calibration

All data were retrieved from the archive and processed with standard data reduction procedures using IRAF[2] tasks. The procedure is briefly described here. We obtained master bias and flat frames (one per filter) for each observing night. Individual frames were bias-subtracted, flattened, shifted to match one another, and combined, after rejecting pixels affected by cosmic ray hits. To combine the frames we imposed no sub-pixel registration, in order to avoid the contamination to SBF due to the sub-pixel interpolation (Jensen et al. 1998). Finally, the seeing between targets and filters ranged between 0.″8 and 1.″0. The combined frames are shown in Fig. 1.

The standard calibration plan of FORS2 provides nightly multi-band observations of Landolt (1992) standards, which were used to calibrate the photometry of the two galaxies.

### 2.2. Data analysis and SBF measurements

To derive the photometry of sources in the frames and measure the fluctuation amplitudes, we used the same procedure as described in our previous works (Cantiello et al. 2005, 2007a,b, 2009; Biscardi et al. 2008). The main steps of SBF measurement involve: sky background determination, model, and large-scale residual subtraction; photometry and masking of point-like and extended sources, including dust; power spectrum analysis of the residual frame.

Here we briefly describe some relevant parts of the analysis. We determined the sky background in the galaxy images by fitting the surface brightness profile of the galaxy with a Sersic's law (Sersic 1968) and a constant term. A first model of the galaxy was obtained and subtracted from the sky-subtracted frame. The wealth of bright sources appearing after model subtraction were masked out. The procedure of model fitting and masking was then iteratively repeated until the residual frame (original frame minus galaxy model) was considered satisfactory. After subtracting of the best galaxy model, the large-scale

[2] IRAF is distributed by the National Optical Astronomy Observatories, which are operated by the Association of Universities for Research in Astronomy, Inc., under cooperative agreement with the National Science Foundation.

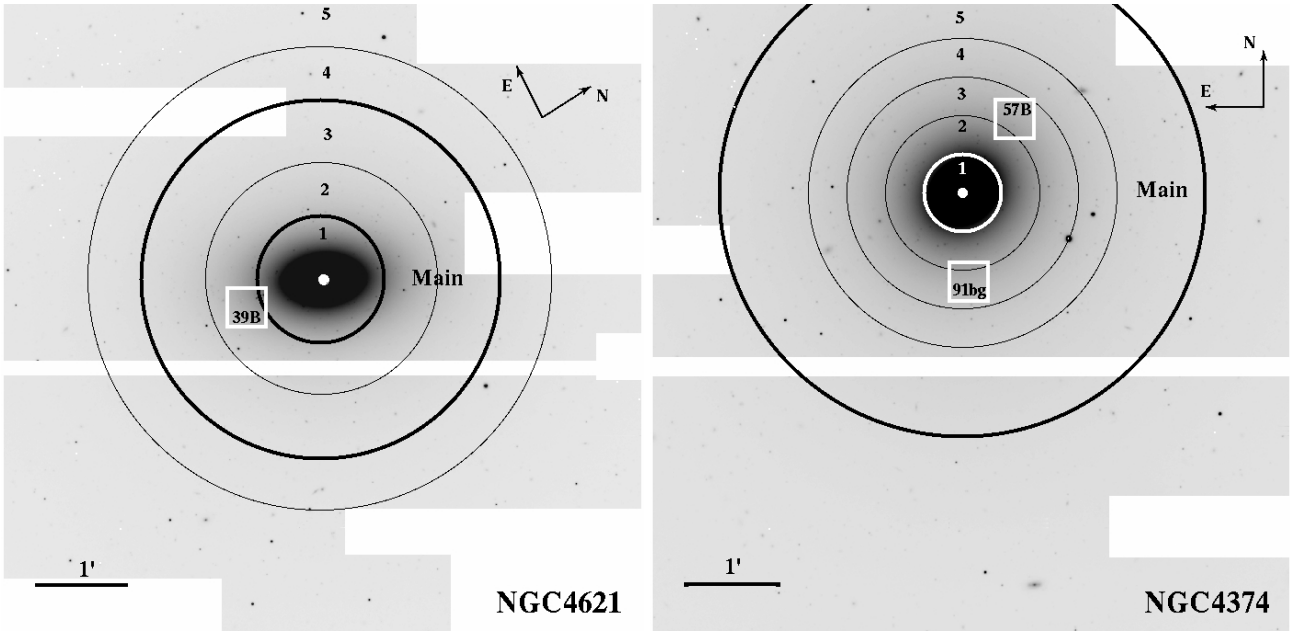


**Fig. 1.** *Left panel*: NGC 4621 *V*-band image with the regions used for SBF and colour analysis. Thick-lined circles mark the borders of the main annulus, thin solid lines show the other annuli (as numbered), white boxes give the location of the SNe (see Sect. 2.2). *Right panel*: like *the left*, but for NGC 4374 (for sake of clarity the inner border of the main annulus is shown in white).

residuals still present in the frame were removed using the background map obtained with SExtractor (Bertin & Arnouts 1996), adopting a mesh size ∼10 times the FWHM (Cantiello et al. 2005). In the following we refer to the image after the subtraction of the sky, galaxy-model, and large-scale residuals as a *residual* frame.

The photometry of fore/background sources and of globular clusters (GCs) was derived with SExtractor on the final residual frame. As described in our previous works, we modified the input weighting image of SExtractor by adding the galaxy model times a factor between 0.5 and 10, depending on the galaxy (for details see Jordán 2004; Cantiello et al. 2005), so that the SBFs were not detected as real objects. To correct for Galactic reddening, we used the $E(B-V)$ values from Schlegel et al. (1998) reported in Table 1. The aperture correction (a.c.) was obtained from several isolated point-source candidates in the frames and from a curve growth analysis out to 6.0″.

Once the corrected catalogue of sources has been derived, the next step was to fit the luminosity functions of external sources, which is used to estimate the extra-fluctuation term due to unmasked faint sources (Tonry et al. 1990). We derived the fit to GCs and background galaxies luminosity functions from the photometric catalogue of sources, after removing the brightest/saturated point-like sources and the brightest and most extended objects. The best-fit of the sum of the two luminosity functions, shown in Fig. 2, and the extra-fluctuation correction term, $P_r$ (see below), were derived as in Cantiello et al. (2005).

To measure SBF magnitudes we proceeded by estimating the azimuthal average of the residual frame power spectrum, $P(k)$, then matching it with the power spectrum of a template PSF convolved with the mask image, $E(k)$. The total fluctuation amplitude $P_0$ was obtained via a robust minimisation method (Press et al. 1992) as the multiplicative factor required to obtain the matching $P(k) = P_0 \times E(k) + P_1$, where $P_1$ is the constant white noise term. For the template PSF, we used six different isolated bright point-like sources in each residual frame, which,

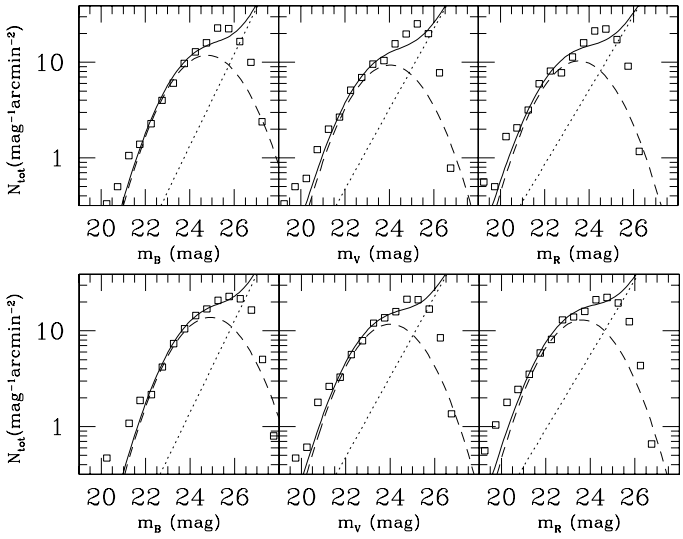


**Fig. 2.** *B*, *V*, and *R* luminosity functions of external sources in NGC 4621 (*upper panels*) and NGC 4374 (*lower panels*). Open squares mark observational data, and the solid lines the best-fit to data. The luminosity functions of background galaxies and GCs are plotted as dotted and dashed lines, respectively.

after normalisation, were singularly adopted to estimate the SBF signal of the galaxy.

For both objects, the fluctuation amplitude, $P_f = P_0 - P_r$, was estimated within a circular annulus, by adopting the same average inner and outer radii used by Tonry et al. (2001) in order to allow a homogeneous combination of ours and the Tonry et al. data. Figure 3 shows the power spectrum analysis of both galaxies.

Furthermore, to study the radial variation of SBFs and the SBF properties at the sites where type Ia supernova events are recorded, we ran the same SBF measurement procedure described above in five annuli per galaxy and in three more

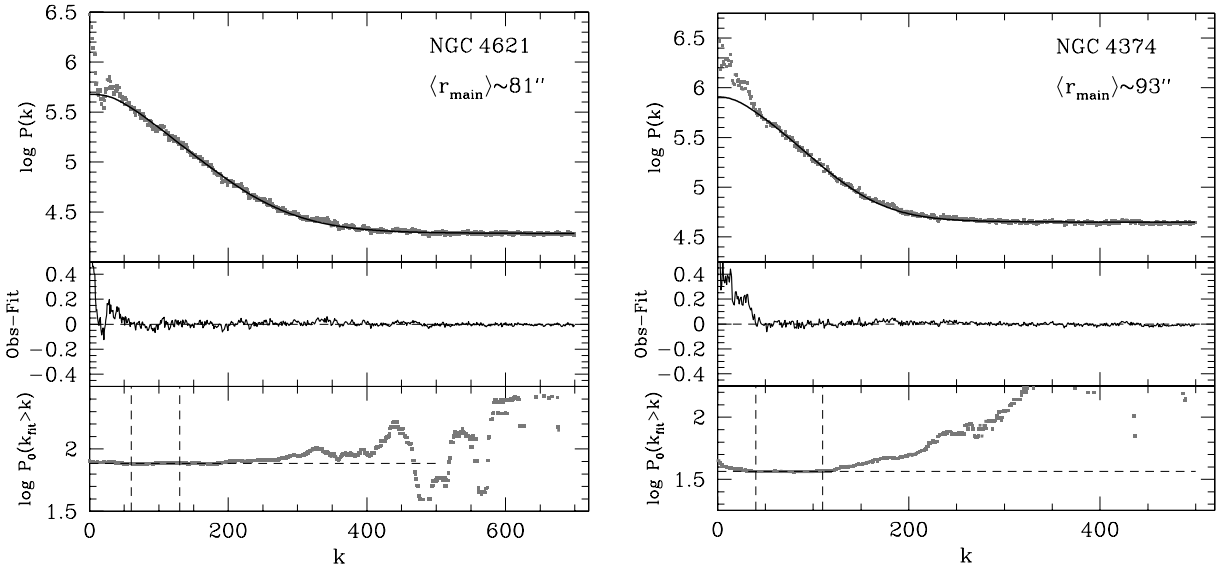


**Fig. 3.** Power spectrum analysis of the main annuli for both targets. *Left panels*: NGC 4621 analysis. *The upper panel* shows the logarithm of the power spectrum of the residual frame (grey dots) and the best-fit $P(k)$ curve (black solid line). In middle panel the difference between observed and fitted data is shown. The flat region of log $P_0(k_{\rm fit} > k)$ between vertical dashed lines in *the lower panel* is used to evaluate the best-fit parameters $P_0$, and $P_1$ (Cantiello et al. 2005; Biscardi et al. 2008). *Right panels*: as left, but for NGC 4374.

**Table 2.** $\langle P_{\rm r}/P_0 \rangle$ ratios (in %).

| | *B* | *V* | *R* | *B* | *V* | *R* |
|---|---|---|---|---|---|---|
| Annulus | NGC 4621 | | | NGC 4374 | | |
| Main | 17 | 7 | 5 | 29 | 11 | 9 |
| 1 | 6 | 4 | 4 | 11 | 7 | 8 |
| 2 | 13 | 6 | 4 | 17 | 9 | 8 |
| 3 | 24 | 9 | 6 | 26 | 11 | 9 |
| 4 | 34 | 13 | 8 | 38 | 13 | 9 |
| 5 | 37 | 15 | 10 | 44 | 16 | 11 |
| SN 1939B | 12 | 5 | 4 | | | |
| SN 1991bg | | | | 37 | 10 | 9 |
| SN 1957B | | | | 25 | 9 | 7 |

box-shaped regions centred on each SN. All regions used are shown in Fig. 1. We must emphasise that the effect of the extra-fluctuation correction term, $P_{\rm r}$, and its relative amplitude with respect to the total fluctuation signal, $P_0$, changes from region to region, and the $P_{\rm r}/P_0$ ratio increases for outer regions and bluer bands. Thus, a systematic under/over-estimate of $P_{\rm r}$ may lead to over/under-estimated SBF magnitudes. Table 2 shows the $\langle P_{\rm r}/P_0 \rangle \times 100$ ratios for all regions and bands considered here; the numbers in the table demonstrate that $V$ and $R$-band SBF magnitudes have much lower $P_{\rm r}$ corrections than the total fluctuation signal, even for the outermost annulus considered. In contrast, for $B$-band measures the $P_{\rm r}/P_0$ ratio in some of the regions considered reaches values as high as ~0.45, implying that the extra correction term is comparable to $P_{\rm f}$, so the SBF magnitudes will be considered with caution in these regions.

Table 3 summarises our measurements; for each galaxy, we tabulated (1) region identification; (2) average equivalent radius of the region $r$(arcsec) $= \sqrt{(ab)}$; (3–5) SBF magnitudes measured in $BVR$, and (6–7) integrated colours.

## 3. Analysis of distances

To estimate distances based on the SBF method a calibration of the absolute SBF magnitude is required, as for most distance indicators. The most widely adopted bands for SBF measurements are the optical $I$ and $z$ bands and the near-IR $H$ and $K$ ones (Pahre & Mould 1994; Tonry et al. 2001; Mei et al. 2007; Jensen et al. 2003; Blakeslee et al. 2010). All $z$ and $H$ measures available come from HST observations taken with the ACS/WFC and NICMOS/NIC2 detectors, respectively (e.g., Jensen et al. 2003; Mei et al. 2007; Blakeslee et al. 2009). The total number of SBF data points available in these pass-bands is around ~450. As a consequence, the calibrations in such bands, especially the optical ones, are well established as testified, for example, by the accurate characterisation of the $\bar{z}$ versus $(g{-}z)$ relation derived by Blakeslee et al. (2009) using ACS data of Virgo and Fornax cluster galaxies.

SBF measurements in other bands are not common, with a total of ~70 measures available for $B$, $V$, and $R$ bands (e.g., Tonry et al. 1990; Jerjen et al. 2000; Blakeslee et al. 2001; Sodemann & Thomsen 1996; Cantiello et al. 2007b). This is because SBF magnitudes at these wavelengths are fainter and tend to be more sensitive to stellar population properties, and consequently the calibration has a larger scatter and is less reliable, while for distance studies the most favourable condition is that the magnitude of the standard candle is relatively constant or has a tight predictive relation as a function of some other distance-independent property, such as colour. Taking advantage of the well-constrained distances of the target galaxies, we derived new distances based on our measurements and empirical/theoretical calibrations, and compared the various results to test calibrations adopted. In the upper part of Table 4 we report the SBF measures for NGC 4621 and NGC 4374 in different bands as derived in literature, the distance moduli $m-M$, and the calibration used. The second part of the table gives the distances derived by us as discussed below.

### 3.1. Empirical calibrations

Cantiello et al. (2007a) compared the existing $I$ and $V$ band calibration equations derived from different observational data sets, in order to identify the best empirical calibration for the colour interval $0.85 \leq V{-}I \leq 1.30$ mag in both pass-bands. For

**Table 3.** Surface brightness fluctuations and colour measurements corrected for galactic extinction.

| Annulus | $\langle r \rangle$ (arcsec) | $\bar{B}$ (mag) | $\bar{V}$ (mag) | $\bar{R}$ (mag) | $B-V$ (mag) | $B-R$ (mag) |
|---|---|---|---|---|---|---|
| | | | NGC 4621 | | | |
| Main | 81 | 32.83 ± 0.10 | 31.84 ± 0.06 | 30.94 ± 0.08 | 0.893 ± 0.002 | 1.449 ± 0.002 |
| 1 | 29 | 32.43 ± 0.09 | 31.75 ± 0.07 | 30.96 ± 0.06 | 0.912 ± 0.001 | 1.474 ± 0.001 |
| 2 | 58 | 32.83 ± 0.10 | 31.83 ± 0.06 | 30.94 ± 0.08 | 0.900 ± 0.001 | 1.455 ± 0.001 |
| 3 | 95 | 32.83 ± 0.10 | 31.81 ± 0.06 | 30.93 ± 0.07 | 0.884 ± 0.002 | 1.439 ± 0.003 |
| 4 | 132 | 32.87 ± 0.11 | 31.74 ± 0.07 | 30.90 ± 0.08 | 0.871 ± 0.005 | 1.431 ± 0.006 |
| 5 | 193 | 32.63 ± 0.12 | 31.59 ± 0.06 | 30.81 ± 0.06 | 0.839 ± 0.008 | 1.391 ± 0.011 |
| SN 1939B | 55 | 33.01 ± 0.10 | 31.84 ± 0.07 | 30.97 ± 0.08 | 0.915 ± 0.001 | 1.469 ± 0.001 |
| | | | NGC 4374 | | | |
| Main | 93 | 33.31 ± 0.08 | 32.11 ± 0.04 | 31.40 ± 0.08 | 0.925 ± 0.002 | 1.494 ± 0.003 |
| 1 | 20 | 32.43 ± 0.06 | 31.51 ± 0.04 | 31.01 ± 0.08 | 0.945 ± 0.001 | 1.521 ± 0.001 |
| 2 | 39 | 33.08 ± 0.07 | 32.03 ± 0.04 | 31.33 ± 0.08 | 0.931 ± 0.001 | 1.501 ± 0.002 |
| 3 | 63 | 33.36 ± 0.09 | 32.23 ± 0.03 | 31.45 ± 0.08 | 0.922 ± 0.002 | 1.489 ± 0.004 |
| 4 | 88 | 33.58 ± 0.08 | 32.23 ± 0.02 | 31.41 ± 0.08 | 0.919 ± 0.003 | 1.486 ± 0.006 |
| 5 | 122 | 33.47 ± 0.10 | 32.22 ± 0.03 | 31.44 ± 0.08 | 0.919 ± 0.006 | 1.486 ± 0.011 |
| SN 1991bg | 58 | 33.87 ± 0.07 | 32.13 ± 0.04 | 31.43 ± 0.08 | 0.927 ± 0.002 | 1.495 ± 0.00 |
| SN 1957B | 59 | 33.50 ± 0.09 | 32.13 ± 0.03 | 31.35 ± 0.08 | 0.917 ± 0.002 | 1.484 ± 0.00 |

**Table 4.** Galaxy distances from this work and from the literature.

| | | | NGC 4621 | | NGC 4374 | |
|---|---|---|---|---|---|---|
| Filter | Colour | Ref. Colour/Data | $\bar{m}$ | $m-M$ | $\bar{m}$ | $m-M$ |
| | | | SBF from literature | | | |
| $I$ | $V-I$ | [1] | 29.67 ± 0.18 | 31.16 ± 0.20 | 29.77 ± 0.09 | 31.16 ± 0.11 |
| $z$ | $g-z$ | [2] | 29.12[a] ± 0.01 | 30.86 ± 0.07 | 29.53[a] ± 0.01 | 31.34 ± 0.07 |
| $K$ | ... | [3] | 25.46 ± 0.16 | ... | 25.43 ± 0.22 | ... |
| | | | Our measurements | | | |
| | | | Empirical calibrations[b] | | | |
| $V$ | $V-I$ | [4] | 31.84 ± 0.06 | 30.91 ± 0.21 | 32.11 ± 0.04 | 31.08 ± 0.20 |
| $R$ | $B-R$ | [5] | 30.94 ± 0.08 | 31.05 ± 0.21 | 31.40 ± 0.08 | 31.25 ± 0.22 |
| | | | Theoretical calibrations-SSP[b] | | | |
| $B$ | $B-R$ | [6] | 32.83 ± 0.10 | 30.2 | 33.31 ± 0.08 | 30.5 |
| $V$ | $B-R$ | [6] | 31.84 ± 0.06 | 30.76 ± 0.21 | 32.11 ± 0.04 | 30.91 ± 0.20 |
| $R$ | $B-R$ | [6] | 30.94 ± 0.08 | 30.93 ± 0.21 | 31.40 ± 0.08 | 31.27 ± 0.22 |
| | | | Theoretical calibrations-CSP[b] | | | |
| $V$ | $V-I$ | [7] | 31.84 ± 0.06 | 30.99 ± 0.21 | 32.11 ± 0.04 | 31.17 ± 0.20 |
| $R$ | $V-I$ | [7] | 30.94 ± 0.08 | 31.04 ± 0.21 | 31.40 ± 0.08 | 31.41 ± 0.22 |
| | | | Median $m-M$ | | | |
| | | | NGC 4621 | | NGC 4374 | |
| | This work | | 30.96 ± 0.11 | | 31.21 ± 0.17 | |
| | all SBFs | | 31.08 ± 0.19 | | 31.21 ± 0.14 | |
| | No SBFs | | 30.97 ± 0.21 | | 31.17 ± 0.18 | |
| | All available $m-M$ | | 30.98 ± 0.17 | | 31.22 ± 0.16 | |

**Notes.** [(a)] Blakeslee et al. (2009) data are given in the AB-mag system. [(b)] We adopted ~0.2 mag as safe calibration error for i) distance moduli given in the literature with no calibration uncertainty; and ii) distances based on theoretical calibrations (see text).
**References.** [1] Tonry et al. (2001); [2] Blakeslee et al. (2009); [3] Pahre & Mould (1994); [4] Cantiello et al. (2007a); [5] Jerjen et al. (2004); [6] this work; [7] Blakeslee et al. (2001).

$V$-band SBF magnitudes, the best calibration equations are:

$$\bar{M}_V = 0.81 \pm 0.12 + (5.3 \pm 0.8) \cdot [(V-I) - 1.15] \quad \text{for } 1.05 \leq V-I \leq 1.30 \text{ mag}; \tag{1}$$

and

$$\bar{M}_V = -0.50 \pm 0.27 \text{ mag for the } 0.85 \leq V-I \leq 1.05 \text{ mag}. \tag{2}$$

To use the above calibration we adopt the $V-I$ colours from Tonry et al. (2001), and the SBF measures listed in Table 3 for the main annulus. These distances are shown in Table 4 and are discussed with all other estimates at the end of the section.

For $R$-band SBF, the most recent empirical calibration for normal elliptical galaxies, was provided by Tonry et al. (1990) who, however, considered it unreliable. Distance estimates for a large number of dwarf ellipticals have been provided by Jerjen and collaborators (e.g., Jerjen et al. 1998, 2000, 2004) based on $R$-band SBF measurements and semi-empirical relations. Using the $B-R$ colour, the authors recognised two different branches

for the SBF versus colour relation, a linear branch:

$$\bar{M}_R = -8.94 + 6.09 \cdot (B{-}R) \text{ for } 1.10 \leq B{-}R \leq 1.50 \text{ mag}; \quad (3)$$

and an parabolic branch, partly overlapping to the previous one (Jerjen et al. 2004):

$$\bar{M}_R = -1.39 + 1.89 \cdot [(B{-}R) - 0.77]^2 \text{ for } 0.80 \leq B{-}R \leq 1.35 \text{ mag}. \quad (4)$$

To derive distances, reported in Table 4, we used the red/linear branch calibration.

The small amplitude of the fluctuations in the $B$-band and the higher sensitivity to stellar population properties with respect to other optical bands (see, e.g., Worthey 1993a; Cantiello et al. 2003, 2007b) make this band unreliable for distances studies. Besides, only a handful of $\bar{B}$ measures exist, including the present ones, and no distance has been estimated using $B$-band SBF measurements.

### 3.2. Theoretical calibrations

Empirical calibrations are generally preferred for SBF studies, also thanks to the aforementioned small uncertainties for certain filters. However, deriving such relations requires substantial observational effort for each pass-band. On the other hand, models have the advantage of being homogeneous through the different bands, but need many different counter-checks to be considered reliable. In this work we take as reference the SBF versus colour equations derived using the simple stellar population (SSP) models from the Teramo-stellar population tools (SPoT) group[3]. For a detailed review of the SPoT models we refer the reader to Raimondo et al. (2005) and references therein. These models have already been proved very effective, not only for matching the empirical SBF calibrations in different bands, but also for reproducing the resolved (colour magnitude diagrams) and unresolved (colours, magnitudes) properties of stellar populations (Brocato et al. 2000; Cantiello et al. 2003, 2007a, 2009; Raimondo et al. 2005; Biscardi et al. 2008; Raimondo 2009).

For example, in a previous paper, Biscardi et al. (2008) showed that the SPoT models for an age interval between 1.5 and 14 Gyr, and metallicity [Fe/H] between –0.4 and 0.3 dex are able to reproduce both the $I$-band and $z$-band calibrations from Tonry et al. (2001) and Mei et al. (2007), respectively.

In the present work we have adopted the same models as used by Biscardi et al. and derived absolute $V$ and $R$-band SBF magnitudes versus the integrated $B{-}R$ colour. Using the on-line SPoT models we obtain the following relations:

$$\bar{M}_R = -4.11 + 2.84 \cdot (B{-}R), \quad (5)$$

$$\bar{M}_V = -2.69 + 2.60 \cdot (B{-}R). \quad (6)$$

We also derive, for sake of completeness, the $B$-band calibration:

$$\bar{M}_B = -0.68 + 2.32 \cdot (B{-}R). \quad (7)$$

However, we recall that it is hazardous to derive distance from Eq. (7) because $\bar{M}_B$ strongly depends on the properties of the stellar population that generates SBF signal (see Sect. 4.1).

As a further check based on an independent set of stellar population models, we also used the $V$ and $R$ equations provided by Blakeslee et al. (2001), which unlike the SPoT models, are derived from composite stellar populations (CSP, see their paper for more details). The distance moduli of the two targets, obtained using both the SPoT and the Blakeslee et al. (2001) theoretical calibrations, are reported in Table 4.

### 3.3. Results

By inspecting the new and old distance estimates in Table 4 we find satisfactory agreement within the quoted uncertainties, regardless of the calibration (empirical or theoretical) or pass-band/colour relation used, with the sole exception of $B$-band data, which we report here only for the sake of completeness.

The distance moduli derived from SBF are affected by the uncertainties present in the empirical/theoretical calibrations, besides the uncertainty of the SBF measure itself. In this work, for the distance moduli taken from the literature where no calibration error is given, we consider it safe to assume an error of ∼0.20 mag, which includes zero-point uncertainty and the scatter of empirical calibrations (Tonry et al. 2001; Jensen et al. 2003). Similarly, we assume ∼0.20 mag error for the theoretical calibrations, which is caused by the spread between models with different ages and metallicities.

Keeping this uncertainty in mind and the error in the SBF measures, the results in Table 4 can be summarised as follows.

- Although the colour provided by Tonry et al. was measured in galaxy regions slightly different from ours[4] the distances derived from $\bar{V}$ using Eq. (1) agree with other data from the literature. A similar result is true for $\bar{R}$ if the linear branch relations by Jerjen et al. (2004) are adopted;
- The distance estimates obtained using empirical calibrations show a slight tendency to have a smaller scatter with respect to those from theoretical calibrations;
- Whether SSP models from the SPoT group or the Blakeslee et al. (2001) composite models are used, the derived distances are very similar to each other and agree with expected values. This result implies that, for the bandpasses and the colour interval considered here, composite stellar population models, which try to better reflect the real population mixing of galaxies, are not strictly necessary for the purposes of deriving appropriate SBF versus colour relations;
- As discussed above, coupling $\bar{B}$ measures with Eq. (7) provides unreliable distance moduli, and this confirms that this band must discarded for distances. Interestingly, the difference between the $B$-band distance moduli and the literature average moduli is significantly greater for NGC 4621 ($\Delta(m-M) = (m-M)_{B,\mathrm{SBF}} - \langle m-M\rangle_{\mathrm{lit.}} \sim -0.8$ mag) than for NGC 4374 ($\Delta(m{-}M) \sim -0.6$ mag). We analyse this evidence further in the next section on stellar population analysis.

Finally, the last lines of Table 4 provide the median distance moduli of the two targets obtained by averaging i) our estimates (empirical and theoretical calibrations, except $B$-band); ii) all SBF $m{-}M$ including ours; iii) the distance moduli without SBF[5];

[3] Visit the web-site: http://www.oa-teramo.inaf.it/spot

[4] As explained before, we adopted the same "average" inner and outer radii as in Tonry et al., but the detailed shape of the annulus, plus the masking of sources, is clearly different between the two data sets.

[5] All non-SBF distances are taken from the NED Redshift Independent Distance database. The distance indicators used include globular cluster and planetary nebulae luminosity functions, type Ia supernovae and globular cluster half light radii. For a complete list of methods and associated references, visit the URL http://ned.ipac.caltech.edu/forms/d.html. In case of multiple estimates obtained with the same indicator, only the most recent one is considered.

and iv) the results from ours plus all literature data. By inspecting these data, we find an excellent agreement between ours and the literature distance moduli, and more generally between non-SBF and SBF-based distances, a result that should be regarded as direct evidence of the absence of any significant bias or systematics between the quoted distances. In addition, such agreement also proves the reliability of $V$- and $R$-band SBF calibrations presented in this section.

### 3.4. Comparison with SNe Ia distances

The comparison of SBF and SNe Ia distances plays a fundamental role in solving the problem of the cosmological distance scale. SBF magnitudes are capable of providing distances with $\lesssim$10% accuracy within 100 Mpc (Jensen et al. 2001; Biscardi et al. 2008; Blakeslee et al. 2010), a result that will be likely improved with new, next-generation observing facilities, allowing an estimate of accurate distances of bright ellipticals out to ~200 Mpc. On the other hand, SNe Ia can provide distances to objects at much greater distances. Thus, deriving self-consistent distances using these two indicators is a crucial step toward bridging local to cosmological distances, to reduce the number of steps in the cosmological distance scale, i.e., to reduce systematic uncertainties.

The sample of objects with known SBF measures and well studied SNe Ia light curves is relatively small, because SNe Ia occur in all kinds of galaxies, but are mostly observed in late type galaxies because of an observational bias; in contrast, SBF are measured almost only in early type galaxies.

Nevertheless, a comparison of SBF and SNe Ia distances was carried out by Ajhar et al. (2001), who find that there is good agreement between the two distance indicators, provided that a consistent set of Cepheid calibrating galaxies is used. However, their statistics are grounded on ~10 objects, and Ajhar et al. make it clear that *"[...] Unquestionably, the SN Ia and SBF absolute calibrations are in need of further refinement."*

As already mentioned, a total of three type Ia supernova events has been recorded in the two galaxies. Two SN Ia have been observed in NGC 4374, SN 1991bg, and SN 1957B, while SN 1939B was discovered in NGC 4621. The SNe are located all at ~1 arcmin from the photometric centre of the host galaxy. Even though all three SNe are classified as type Ia, they show a wide range of luminosity, as expected in E/S0 galaxies (Gallagher et al. 2005); in particular, all events are fainter at maximum light than a normal SN Ia after correcting for the correlation between peak luminosity and decline rate (Hamuy et al. 1996). SN 1991bg is one of the most sub-luminous SN Ia yet observed (~2.5 mag fainter than normal, Turatto et al. 1996). SN 1957B has an absolute magnitude at maximum ~0.2 mag fainter than a normal SN, but still brighter than SN 1991bg (Howell 2001). Finally, SN 1939B at maximum light is ~0.6 mag sub-luminous (Minkowski 1964).

Unfortunately, because they are sub-luminous events, the standard peak luminosity versus decline rate relation does not provide good distance estimates with these SNe. Ajhar et al. (2001), in fact, did not take SN 1939B and SN 1957B into account, while SN 1991bg appears in their list of supernovae, though it was used not for the SBF-SNe Ia comparison, but instead was included *"for completeness and for future studies of SNe Ia luminosities"*.

More recent studies, however, have provided new methods that can be adopted to derive distances with these sub-luminous SNe: the calibration based on decline rate and colours by Folatelli et al. (2010), the MLCS2k2 by Jha et al. (2007), and the $\Delta C_{12}$ method by Wang et al. (2006).

Using Eq. (6) of Folatelli et al. (2010) with the best-observed fit parameters, we obtain the following distance moduli:

- SN 1939B in NGC 4621: taking the peak luminosity from the Asiago Supernova Catalogue (Barbon et al. 1989)[6] $m_{B,\max} = 12.3$, a decline rate of $\Delta m_{15} \sim 1.75$ estimated from the light curve reported in Leibundgut et al. (1991), and Eq. (3) from Folatelli et al. (2010) to get the $(B^{\max} - V^{\max})_0$ colour, we obtain $m - M = 31.0$, with an uncertainty of ~0.5 mag if errors of ~0.2 mag, 0.25 days, and 0.15 mag are adopted for $m_{B,\max}$, $\Delta m_{15}$, and $(B^{\max} - V^{\max})_0$, respectively;
- SN 1957B in NGC 4374: adopting $m_{B,\max} = 12.20 \pm 0.14$ (Lanoix 1998), $\Delta m_{15} = 1.3$ (Howell 2001), and $(B^{\max} - V^{\max})_0 = 0.01$ (using Eq. (3) from Folatelli et al. 2010), the distance modulus is $m - M = 31.1$, with uncertainty ~0.3 mag when adopting an error of ~0.1 on both the decline rate and $(B^{\max} - V^{\max})_0$;
- SN 1991bg in NGC 4374: with $m_{B,\max} = 14.75$ and $m_{V,\max} = 13.95 \pm 0.02$ (Turatto et al. 1996), and $\Delta m_{15} = 1.93 \pm 0.10$ (Phillips et al. 1999), we derive $m - M = 31.1 \pm 0.3$.

In all cases, the distance moduli derived using the calibration from Folatelli et al. (2010) agree within uncertainties with the median values reported in Table 4.

Jha et al. (2007) have developed an updated version of the MLCS method (Riess et al. 1998) called MLCS2k2, which includes new procedures for the $K$-correction and for internal extinction corrections. Using the light curve parameters of SN 1991bg, Jha et al. derive $m - M = 31.42 \pm 0.10$, adopting $H_0 = 65$ Km s$^{-1}$ Mpc$^{-1}$. Although such a distance agrees with the values reported in Table 4, the agreement certainly becomes better if $H_0 = 73$ Km s$^{-1}$ Mpc$^{-1}$ is taken, a value consistent with the ones typically derived from SBF distances (Tonry et al. 2000; Freedman et al. 2001), as suggested by the authors. In that case, in fact, one has $m - M = 31.17 \pm 0.10$ mag.

In Wang et al. (2006), the adopted calibration parameter is the $\Delta C_{12}$, i.e., the $B-V$ colour at 12 days past optical maximum. The authors find $m - M = 30.35 \pm 0.19$, based on the properties of SN 1991bg and using $H_0 = 72$ Km s$^{-1}$ Mpc$^{-1}$. This $m - M$ is more than 2-$\sigma$ from the median values in Table 4 which were obtained using many independent distance indicators, and it also disagrees with the values obtained from the Folatelli et al. (2010) or Jha et al. (2007) calibrations, so we flag the Wang et al. estimate as unreliable for the case of SN 1991bg.

In conclusion, we find that the distances of NGC 4621 and NGC 4374 derived via the light curve properties of their SN Ia agree perfectly with the SBF distances – and with the most recent estimates from the literature – if the calibration by Folatelli et al. (2010, useful for all three SNe) or Jha et al. (2007, for the case of SN 1991bg) are used.

## 4. Analysis of unresolved stellar populations with SBF and integrated colours

As mentioned, the SBF magnitude of a stellar population corresponds to the ratio of the second to the first moment of its luminosity function. Since its first applications, this characteristic has suggested the use of the SBF method as a powerful diagnostic of stellar population properties. The earliest theoretical studies

[6] The updated catalogue is available at the URL http://graspa.oapd.inaf.it

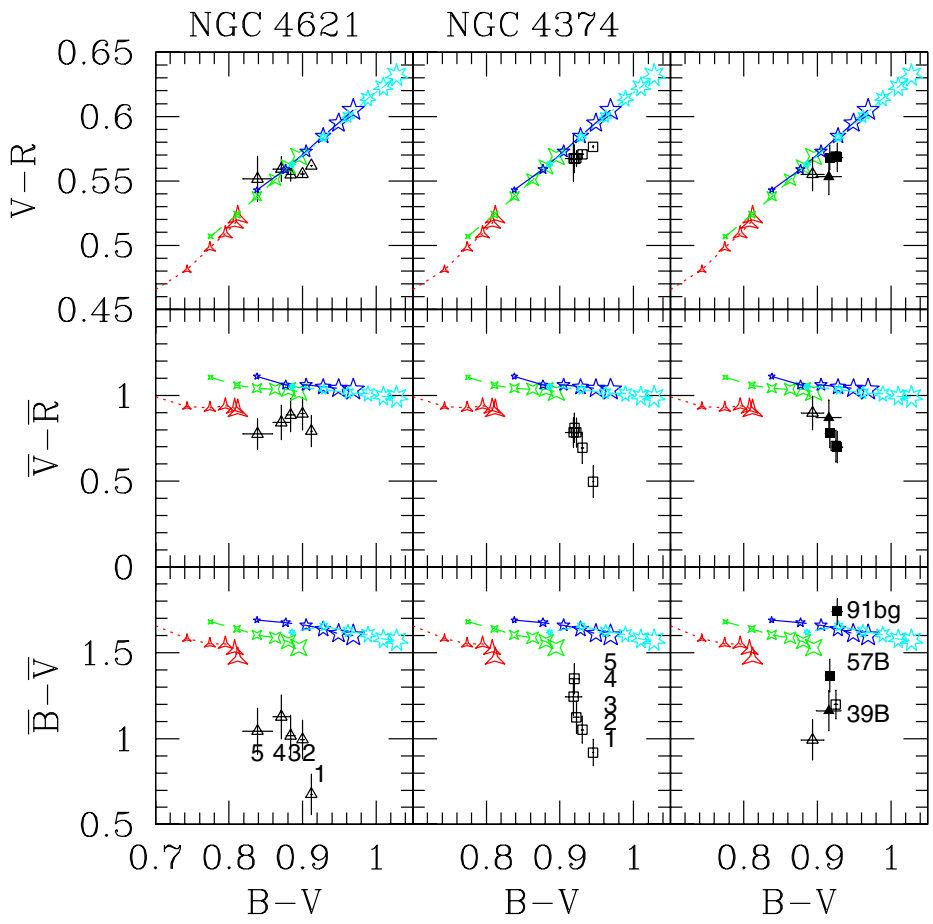


**Fig. 4.** SBF-colours and integrated-colours measured for NGC 4621 (*left panels*) and NGC 4374 (*middle panels*), compared to the SPoT models from Raimondo et al. (in prep.). Black symbols mark observational data for the various annuli as labelled (triangles for NGC 4621, squares for NGC 4374). Measures within regions hosting SNe, and the measure for the main annulus for both galaxies, are shown in *right panels*: NGC 4621 and its SN Ia (SN 1939B) are shown with full and empty triangles, respectively; NGC 4374 and its SNe Ia (SN 1957B, and SN 1991bg) are shown with full and empty squares, respectively. For the models, different [Fe/H] are indicated with different symbols ([Fe/H] = −0.7, –0.4, 0.0, +0.4 dex with three, four, five, and seven pointed stars, respectively). Larger symbols indicate older ages, from 4 to 14 Gyr in 2 Gyr steps (*See electronic version of the Journal for a colour version of the figure*).

on this subject (Buzzoni 1993; Worthey 1993a,b) were focused on the relationship between SBF and age/metallicity, but they also showed how the fluctuation amplitude in bluer pass-bands, like $B$, could be used as a useful tracer of the hot stellar components in the galaxy. Even though several authors have confirmed and extended these early findings (Blakeslee et al. 2001; Cantiello et al. 2003; González et al. 2004; Raimondo 2009), a comprehensive and homogeneous analysis of multi-band SBF measurements for a large sample of galaxies is still lacking. The various sets of models have clearly shown that optical to near-IR SBF colours can be very effective for lifting the age/metallicity degeneracy that affects "classical" integrated colours (Worthey 1994). Observationally, a few $\bar{I}-\bar{H}$ data sets exist in literature (Jensen et al. 2003), but they mostly refer to spatially non homogeneous regions. On the other hand, $\bar{V}-\bar{I}$ colours have also been studied for various galaxies, but they suffer an age/metallicity degeneracy that is similar to classical colours, although the information obtained using such measures is independent and complementary to the integrated colours derived for the same targets (Tonry et al. 1990; Blakeslee et al. 2001; Cantiello et al. 2007a,b).

Concerning the use of SBF to study stellar populations, high-quality data has allowed SBF variations to be measured in optical bands within different regions of the galaxy. As a consequence, even if $V$ and $I$ SBF magnitudes and colours are not as effective in removing the age/metallicity degeneracy (see below), the measure of SBF radial variations has provided useful results on how the mean properties of the dominant stellar population change with galactic radius (Cantiello et al. 2005).

The targets analysed in this work have already been considered for other SBF measurement surveys. In particular, the aforementioned ground-based SBF survey (Tonry et al. 2001), the near-IR measurements for nine Virgo ellipticals by Pahre & Mould (1994), and the ACS Virgo Cluster Survey (Côté et al. 2004), all have both galaxies in their target list. The SBF magnitudes from these databases are reported in the first part of Table 4. None of these cited works presents the measurement of SBF magnitudes at various galactic radii. In contrast, thanks to the high quality of the VLT data available, we have been able to obtain fluctuation amplitudes at various radii (Table 3).

Unlike other bright elliptical galaxies studied in previous works (Cantiello et al. 2005, 2007a), we can report the absence of radial $\bar{V}$ and $\bar{R}$ gradients in NGC 4374. For NGC 4621, instead, a small but non-negligible brightening of SBF magnitudes at larger radii is found in $V$ and $R$. On the other hand, the $\bar{B}$ of both galaxies shows a significant scatter between the different annuli, thus no evidence of systematic trends with radius is observed in this band.

### 4.1. SBF-colours versus integrated colours

By plotting SBF and integrated colours for each target (Fig. 4) and comparing the data of the two galaxies between them and with models, we can offer various considerations about the host's unresolved stellar systems. We consider the updated version of the SPoT models (Raimondo et al., in prep.), which for the photometric bands and chemical composition used in this section confirm the results from the previous Raimondo et al. (2005) models.

As a first general consideration, we find that the SBF $\bar{V}-\bar{R}$ colour and the integrated $B-V$ and $V-R$ colours predicted by models representing old ($\gtrsim$7 Gyr) and metal-rich ([Fe/H] $\gtrsim$ −0.4 dex) SSPs are in good agreement with the measured values. In contrast, the $\bar{B}$ is much more sensitive to the properties of the dominant stellar population (see below), and the match with "canonical" SSP models is less satisfactory in this band.

Starting from these general considerations on the properties of the "dominant" stellar population in the galaxies (i.e., the stellar population which is emitting the largest part for the flux responsible for the colours and the SBF signal) let us analyse the result of Fig. 4 in more details.

The left and middle columns of panels in Fig. 4 show the SBF colours and $V-R$ measurements in the five annuli considered for each galaxy versus the integrated $B-V$. The annuli appear numbered in the lower panels according to the numbers reported in Table 3, so that by inspecting the data in the figure, it is also possible to recognise the radial behaviour of plotted quantities. In the third column, instead, the overall SBF measures are plotted ("main" annulus data in Table 3, empty symbols) together with SBF in the SNe regions. It is useful to emphasise that for both galaxies our integrated colours and colour profiles agree with the same measurements from Idiart et al. (2002).

By inspecting results in the figure, we find that NGC 4621 does not show any significant SBF colour gradient in either $\bar{B}-\bar{V}$ or $\bar{V}-\bar{R}$ (lower and middle left panels), and no gradient even in the integrated $V-R$ colour (top left panel). The only colour showing radial changes is the $B-V$, varying from ∼0.91 mag for the inner annulus (#1), to ∼0.84 in the outermost (#5). As already mentioned, inspecting the $\bar{V}$ and $\bar{R}$ data for NGC 4621 in Table 3, a small but non-negligible gradient seems to be present, ∼0.25 mag in $V$ and ∼0.15 mag in $R$, if the inner annulus is discarded. The $\bar{V}$ and $\bar{R}$ gradients have the same trend with colour, i.e., brighter SBF magnitudes associated with bluer colours/larger radii, thus they tend to cancel out when the SBF colour is considered. In fact, if the innermost annulus is neglected, an SBF-colour gradient appears in the $\bar{V}-\bar{R}$ versus $B-V$ plane for NGC 4621, although it has the same amplitude of estimated uncertainties. Even so, the radial trends of the SBF magnitudes and of the $B-V$ are both consistent with the well known scenario of a more metal-poor stellar component (i.e., bluer integrated colours and brighter SBF magnitudes for the pass-bands considered here) at larger galactocentric radii.

For NGC 4374 (central panels), we find that $\bar{V}-\bar{R}$ and $V-R$ are practically flat along the galaxy radius, if the innermost annulus (#1) is excluded. Owing to the presence of a dusty disk in the galaxy centre, in fact, we left unmasked only a small fraction of the area in the annulus #1, but more contamination from dust might still be present. Unlike the previous case, the $V$ and $R$ data of NGC 4374 in Table 3 do not show any systematicity with radius, although the $\bar{V}-\bar{R}$ versus $B-V$ panel seems to show a correlation between the two plotted magnitudes, mostly due to the cited innermost annulus.

As mentioned above, the comparison between measurements and models in the two upper panels of each column reveals that the data of galaxies lie close to the position of SSPs with [Fe/H] $\gtrsim$ −0.4 dex and $t \gtrsim 7$ Gyr. However the age-metallicity degeneracy suffered by classical and SBF colours that were obtained by combining these bands prevents us from giving more precise information on the dominant stellar components in the galaxy.

The lower panels, which involve $\bar{B}$, deserve a separate and detailed discussion, since both galaxies show a $\bar{B}-\bar{V}$ colour much bluer than models, an evidence more severe for NGC 4621. For this galaxy, in fact, the $(\bar{B}-\bar{V})_{\rm Main}$ is ∼0.2 mag bluer than NGC 4374, and ∼0.4 mag bluer than models. We also note that NGC 4374 shows a radial change leading the $\bar{B}-\bar{V}$ value of the outermost annulus to be quite similar to the models. In contrast, NGC 4621 does not present any systematic gradient and, except for the innermost annulus, the $\bar{B}-\bar{V}$ is nearly constant in every studied region of the galaxy.

To understand the origin of the mismatch between data and models, visible in the lowermost panels of Fig. 4, and of the peculiarly blue $\bar{B}-\bar{V}$ colour of NGC 4621, we considered taking advantage of the versatility of the SPoT stellar population synthesis code to carry out some specific numerical simulations to investigate if and how the presence of a complex stellar population modifies the expected $\bar{B}-\bar{V}$. In addition, for metal-rich models we also considered the case of a non-negligible fraction of horizontal branch (HB) stars having higher effective temperatures with respect to "canonical" stellar evolution models.

In order to find indications of the origin of the peculiar $\bar{B}-\bar{V}$ behaviour of the two galaxies, our numerical tests were organised as follows. 1) We explored the effects of a hot HB (HHB) component on field stars; 2) a young stellar population was added to a "reference" old and metal-rich population; and 3) a metal-poor population was added to the reference one. For the comparison in $B$, $V$, and $R$ bands, we adopted the SBF measured in five annuli, plus the measurement in the SNa Ia regions, while for the panels including the $\bar{K}$ taken from the literature we adopted our main annuli SBF measurements. The results of the simulations and the comparisons with data are briefly discussed below, and shown in Fig. 5 where three different SBF colours are plotted against $B-V$.

- In order to mimic the presence of HHB stars, we carried out a numerical experiment by considering that 50% of HB stars have suffered strong mass loss during the RGB phase (first column of panels in Fig. 5). As a result, a percentage of low-mass stars populates the blue/hot part of the HB. This is realistic since such a hot component is observed in several metal-rich stellar clusters (e.g., NGC 6441 and NGC 6388), regardless of the mechanism responsible for this evidence. In the figure we consider three populations with solar metallicity and ages 10, 12, and 14 Gyr. Both SBF and integrated colours move from the "standard" positions (standard HB, SHB, label in the figure) to the hot/blue region of the diagram (HHB in the figure). The effect is stronger for SBF colours including $\bar{B}$ with respect to integrated colour because of their increased sensitivity to even a few bright hot stars.
- In the second numerical experiment (middle panels), a very young population (two different ages are considered: 30 Myr and 100 Myr) is added to a population of 14 Gyr and solar metallicity, with a mass ratio between the two components $1_{\rm old}{:}10^{-3}_{\rm young}$. From the middle panels of Fig. 5 it appears that a very recent and *diffuse* burst of star formation is required to obtain a good match between models and data.
- The third column of Fig. 5 reports the effects of a secondary metal-poor component of 14 Gyr added to the main solar metallicity one, the [Fe/H] of the metal-poor component are labelled in the lower right panel of the figure. Only a very metal-poor population with a mass comparable to the one of the main component ($1_{\rm m.rich}{:}1_{\rm m.poor}$) produces relevant effects on SBF colours. In that case, however, the values of the observed integrated colour $B-V$ are not reproduced well any more.

The three sets of simulations described seem to point out what has already been suggested: the most likely solution to the puz-

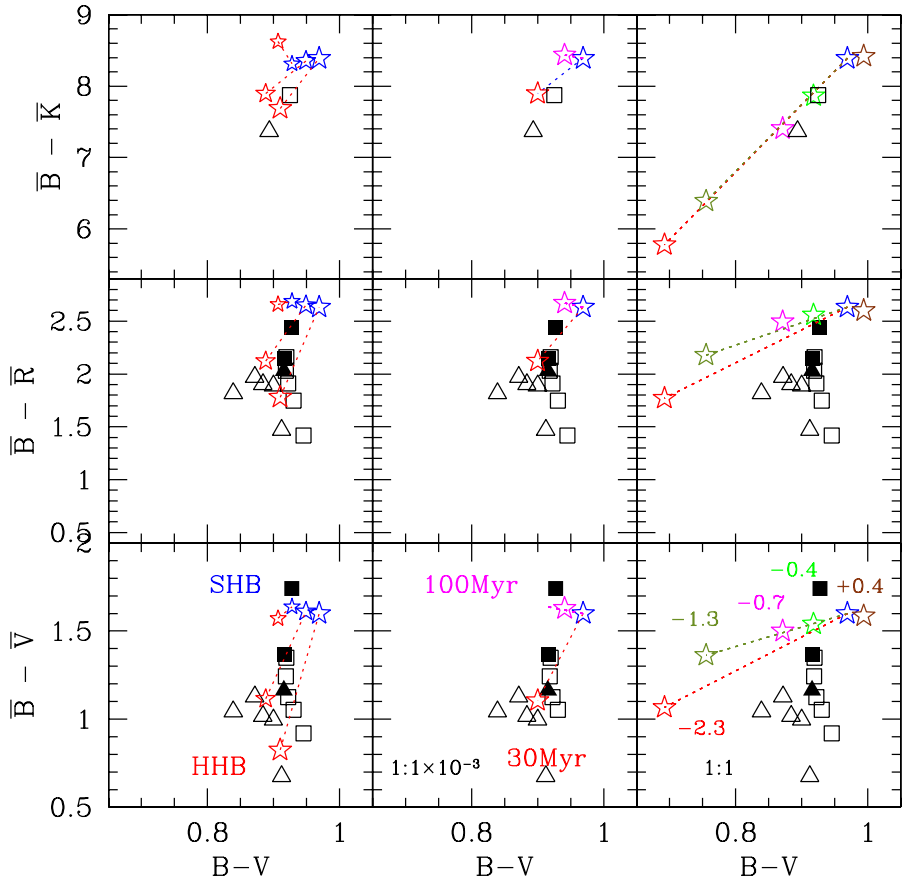


**Fig. 5.** SPoT stellar population models obtained with non-canonical assumptions. In all cases the initial (standard) population has solar metallicity and $t \sim 14$ Gyr, and is shown with a blue star in *each panel*, while the final composite population is shown with a different colour and connected with a dashed line to the reference model. *Upper panels* show main annulus measures, while *middle and lower panels* show multi-annuli measures and SNe Ia regions. *Left panels*: a fraction equal to 50% of the total HB-stars is simulated as HHB. For these models three ages are considered ($t$ = 10, 12, and 14 Gyr increasing ages are marked with larger symbols). *Middle panels*: a young population of $t$ = 30 Myr (red) or $t$ = 100 Myr (magenta) is added to the old solar one. The fraction in mass of old to young stars is reported in *the lower panel*. *Right panels*: various metallicities are added to the solar one, as labelled. The mass fraction metal-poor to standard SSPs is shown in the lower panel. Symbols for observational data are as in Fig. 4 (*See electronic version of the Journal for a colour version of the figure*).

zling behaviour of $B$-band SBF is the presence of hot HB stars. In fact, while the presence of a hot/young stellar component provides a good match between integrated and SBF colours models with data (second scenario, middle panels in Fig. 5), it appears unrealistic that these regular ellipticals host such diffuse and very young stellar components. Moreover, in such a case, i.e., an object with massive and extended recent star formation, it is likely that a large quantity of dust would still be present, preventing measuring the SBF itself. However, with only the exception of an inner $r \lesssim 20''$ dust ring in NGC 4374, we do not find any sign of extended dust in either galaxy. The two-metallicity mixing scenario seems even more unlikely. This mixing, in fact, does not solve the mismatch between data and models for optical bands.

As a further element to support the role played by HHB stars in determining the SBF signal of NGC 4621, we recall the works by Brown et al. (2000, 2008), based on deep near and far-UV images of the compact elliptical galaxy M 32. Using HST data, the authors find that the number of PAGB stars in M 32 is significantly lower than the expectations of their stellar evolution models, while the presence of an HHB population has been observed and identified as the main contributor to the UV-emission of the galaxy.

Related to this issue, Cantiello et al. (2007a), using the $\bar{B}$ data of eight ellipticals, suggest that the role of hot evolved stars cannot be neglected in modelling SBF magnitudes in this passband. In that case, though, the mismatch between the data and models in $\bar{B}$ was solved by enhancing the number of PAGB expected when assuming the evolutionary prescriptions by Brocato et al. (1990, 2000).

For NGC 4621, our present results point towards the direction suggested by the observations of M 32. We show that HHB stars can be the stellar component responsible for the observed $\bar{B}$-excess, even though a combination of two stellar components (HHB and PAGB stars) could not be ruled out, so the topic requires further investigations.

As already mentioned for the case of M 32, another piece of information comes from comparing of the integrated properties of the two galaxies in the wavelength interval where the very hot stellar component is dominant, i.e., the UV regime. In this wavelength regime, Longo et al. (1991) found that NGC 4621 is brighter than NGC 4374. The puzzling presence of a strong UV emission in some regular early-type galaxies, discovered in the late '70s (Code et al. 1972; Bertola et al. 1980), is now widely interpreted as the presence of an old hot stellar component. Although the mechanisms that created such component, or even its true nature, are not well understood (Park & Lee 1997; Kaviraj et al. 2007; Han 2008), some of these old hot stellar sources may have effects on $\bar{B}$, as discussed by various authors based on both SSP models' predictions (Worthey 1993a; Cantiello et al. 2003) or on empirical data (Shopbell et al. 1993; Sodemann & Thomsen 1996; Cantiello et al. 2007a). Moreover, a recent study by Buzzoni & González-Lópezlira (2008) presents a detailed analysis of the link between the UV characteristics and near-IR SBF amplitudes of elliptical galaxies.

In conclusion, the present analysis seems to support a scenario where the peculiar $\bar{B}-\bar{V}$ is related to a hot and old diffuse stellar component, like HHB stars. Larger samples of SBF colours in blue bands are required to provide further constraints.

### 4.2. SBF colour–colour diagrams

The coupling of literature $I$, $z$ and $K$-band SBF data for the two galaxies with our measurements (main annuli) provides a

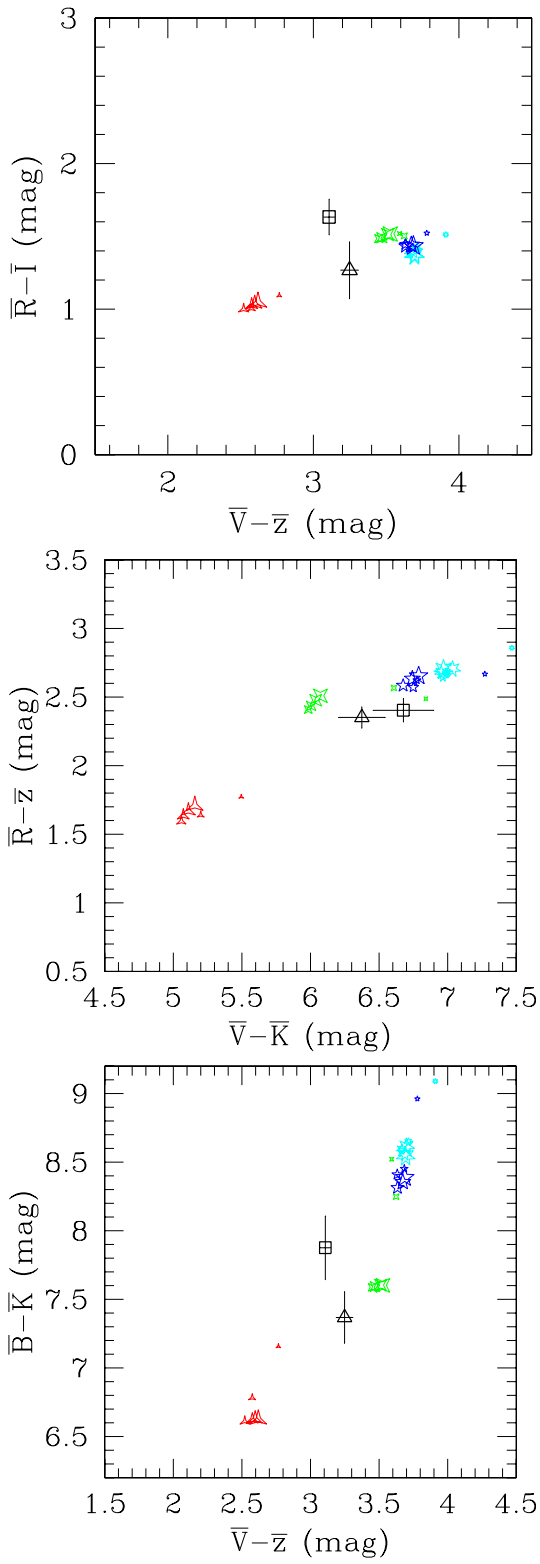


**Fig. 6.** SBF colour–colour diagrams obtained from present measures (main annulus) and literature data. Symbols and models are the same as for Fig. 4. For consistency with other filters, the $z$-band SBF magnitudes given by Blakeslee et al. (2009) are transformed from the ABmag to the Vegamag system according to Sirianni et al. (2005) (*See electronic version of the Journal for a colour version of the figure*).

sample of six independent SBF values useful for obtaining three independent SBF-colour versus SBF-colour diagrams. Such wide pass-band coverage is, to our knowledge, the first ever presented for SBF. The diagrams with observations are shown in Fig. 6, together with models. The upper panel of the figure shows a feature that has already been discussed (e.g., Blakeslee et al. 2001; Cantiello et al. 2003); i.e., that model separation for pure optical SBF colours is not effective in removing the age-metallicity degeneracy. In this panel, in fact, all [Fe/H] $\geq$ –0.4 dex models overlap each other, with old and metal-rich models superposed on young and metal-poor ones.

The model degeneracy is significantly reduced in the middle panel, which includes the optical to near-IR $V-K$ SBF colour. The position of the two objects overlaps with models with different metal contents. In particular, the bluer point, i.e., NGC 4621, is located near the region of [Fe/H] $\sim$ –0.4 dex with respect to NGC 4374, which appears slightly more metal-rich. This behaviour is not unexpected, since the second galaxy is brighter than the first one and, due to the known mass-metallicity relation (e.g., Bernardi et al. 1998), it is reasonable to expect a field population that is slightly more metal-rich in NGC 4374. It is worth emphasising that the two-SBF-colour panel represents a useful tool for providing insights into the "absolute" [Fe/H] of the dominant stellar component, within the observational error bars, and the SSP models scenario adopted.

In other words, based on the SBF-colours analysis and on the integrated colours of field stars from this work (see also Tonry et al. 2001; Idiart et al. 2002; Mei et al. 2007) we find that the dominant stellar population of NGC 4374 is either more metal rich or older, or both, than what is found in NGC 4621. Moreover, this result agrees with independent estimates of the metal content in these galaxies, which are based on spectral index measurements, which predict nearly identical (Idiart et al. 2007) or slightly higher metallicity for NGC 4621 (Kuntschner et al. 2001; Scott et al. 2009).

It must be pointed out, though, that these results are based on the naive interpretation of field stellar population properties solely in terms of age and chemical content differences. Nevertheless, as discussed above, SBF magnitudes and colours can be very sensitive to the presence of a blue/hot stellar sub-system, especially SBF in bluer pass-bands.

The lower panel in Fig. 6 includes our $\bar{B}$ measurements. As for the first panel, the $\bar{V}-\bar{z}$ colour is used in the abscissa, in this case the separation between different SSP models allows recognising that for the two higher [Fe/H] values the $\bar{V}-\bar{z}$ colour is bluer for older ages. Taking the models with solar metallicity as reference, one can conclude that both galaxies have similar $\bar{V}-\bar{z}$, matching the oldest SSP models, but NGC 4621 has $\bar{B}-\bar{K}$ $\sim$ 0.6 mag bluer than NGC 4374, as one would also expect when a diffuse hot stellar component is present in this galaxy. As an example, a canonical SSP model at $t$ = 14 Gyr, solar metallicity has $\bar{B}-\bar{K}$ $\sim$ 8.4 and $\bar{V}-\bar{z}$ $\sim$ 3.7 mag. By artificially increasing the number of HHB stars (as described in Sect. 4.1) our models predict $\bar{B}-\bar{K}$ $\sim$ 7.7, i.e., roughly the $\Delta\bar{B}-\bar{K}$ colour difference between the two galaxies, while $\bar{V}-\bar{z}$ is left unchanged.

A further consideration is that, in the bottom panel of Fig. 6, NGC 4621 falls within the region of models with [Fe/H] between –0.7 and –0.4 dex, even though the $B$-band SBF is too bright. Such behaviour could be explained with bright $K$-band SBF, so that the $B$ and $K$ SBF excesses compensate for each other allowing observations to match models of intermediate metallicity. This would also make $\bar{V}-\bar{K}$ too red, causing the shift observed in the middle panel. In that case, i.e., that $B$ and $K$-band SBF are too bright, the three panels of Fig. 6 all suggest an [Fe/H] $\lesssim$ –0.4 for NGC 4621 and higher metallicity for the dominant stellar component in NGC 4374.

Whether the position of NGC 4621 with respect to models comes from a metal-poor, dominant stellar component, or if it is related to a diffuse hot component, cannot be established with present data. New independent observational data-sets, and accurate modelling that is able to match all the observed properties of the two galaxies are needed to better understand the physical characteristics of the unresolved stellar systems in both targets.

Nevertheless, the coupling of $B$-band with other optical or near-IR SBF measures appears to be a promising method of unveiling the properties of hot stellar components possibly hidden to other photometric indicators.

### 4.3. SBF colours and stellar populations properties in regions hosting type Ia Supernovae

The correlation between the SN Ia peak magnitude and the host-galaxy morphology, i.e., the host stellar population, has been known since the work by Hamuy et al. (1996), which shows that intrinsically fainter events occur in early-type galaxies, while luminous events are often seen in late-type galaxies. The results on the mean stellar population properties in the galaxies, as discussed in the previous sections, seem to support the idea that old stellar system, i.e., old progenitors, are required for sub-luminous SNe Ia.

To better constrain the properties of the *local* stellar populations we measured SBF and colours in the areas where the SNe Ia exploded, adopting a $25'' \times 25''$ square region. The results of the measurements are reported in Table 3 and are shown in the right panels of Fig. 4.

First of all, we note that, from $B{-}V$, $V{-}R$ and $\bar{V}{-}\bar{R}$ data, the stellar population properties in the selected regions and in the main annulus appear remarkably homogeneous. Taking only such colours into account, we conclude that the stellar component in the regions hosting the three SNe Ia and the overall stellar population in the galaxies have very similar properties, with all data matching SSP models of [Fe/H] $\gtrsim -0.4$ dex and $t \gtrsim 7$ Gyr. In any case, old ages are expected, supporting the results by Gallagher et al. (2008) based on spectroscopic data. It is interesting to note that the properties of the dominant stellar populations in the regions of the two SNe Ia host by NGC 4374 appear strikingly similar in these panels, even nearly identical to each other, notwithstanding the large projected separation (~10 kpc) between the two regions.

Larger differences are seen between the three regions in the $\bar{B}{-}\bar{V}$ versus $B{-}V$ panel (lower right panel in Fig. 4). Due to the aforementioned stronger sensitivity of $B$-band SBF to changes in stellar population properties with respect to other pass-bands, the larger scatter between the three SNe Ia is not surprising, and it might possibly be related to different levels of local "pollution" from a hot stellar component. Furthermore, the regions of NGC 4374 where SN 1991bg and SN 1957B exploded show a $\Delta\bar{B}{-}\bar{V} \sim 0.4$ mag, despite their nearly homogeneous $B{-}V$, $V{-}R$, and $\bar{V}{-}\bar{R}$ colours. Whether the $\Delta\bar{B}{-}\bar{V}$ is related to the SNe progenitors and their environment, hence to the $\Delta B_{\rm max} \sim 2.3$ mag between the two SNe Ia, or to problems with the $P_{\rm r}$ correction cannot be said using present data, and further analysis based on a richer sample is needed.

For NGC 4621, even including $B$-band SBF data we find a good matching between global and local, i.e., near SN 1939B, stellar population properties.

## 5. Conclusions

We have presented a detailed multi-band study of SBF magnitudes for two bright galaxies in the Virgo cluster, NGC 4621 and NGC 4374, based on deep $B$, $V$, and $R$-band imaging data of the FORS2 camera at the VLT telescope.

Among the three bands available, the $V$ and $R$ have known empirical SBF calibrations that are useful for obtaining the distances of the targets. Coupling our measurements with these calibrations, or with calibrations obtained from simple and composite stellar population models, we obtained accurate distances for the two galaxies which agree very well with other distance estimates taken from the literature. This demonstrates both the reliability of the measured SBF magnitudes and the goodness of the calibrations adopted. Taking advantage of the availability of various SBF distances for the two targets, based on different calibrations for different filters, we compared the average SBF distance moduli with other non-SBF ones to check for any possible systematics. Although the sample of galaxies is statistically small, the results seem to rule out any possible bias on SBF distances.

Taking the median of all available SBF and non-SBF distance estimates, we estimated $m - M = 30.98 \pm 0.17$ for NGC 4621 and $m - M = 31.22 \pm 0.16$ for NGC 4374. The two target galaxies hosted a total of three SN Ia events: one in NGC 4621, SN 1939B, and two in NGC 4374, SN 1957B and SN 1991bg, all classified as sub-luminous. Using some recent calibration relations based on decline rate and colours of the SN (Folatelli et al. 2010) and on the updated MLCS method (Jha et al. 2007), we find excellent agreement between the SBF and SNe Ia distances. This result is very promising in view of a reduction of the number of "rungs" to bridge local to cosmological scale distances, i.e., to significantly reduce the systematic uncertainties on distances of objects at large distances and, consequently, on cosmological parameters.

We also carried out SBF measurements on $B$-band images, but such measures were rejected for distance analysis. The sensitivity of SBF magnitudes in this band to the stellar population properties makes any calibration in this band unreliable. We tentatively derived a $B$-band calibration based on SPoT models, which have proved realistic in both $V$ and $R$ bands, as well as in the other bands studied (Biscardi et al. 2008), but the results confirm that SBF magnitudes in such a band are not well suited to any kind of distance analysis.

Thanks to the high quality of the data, we have succeeded in measuring SBF magnitudes in various galactic regions. Both integrated and SBF colours (excluding $\bar{B}$) seem to point to the relative uniformity of the stellar population along the galaxy radius. No sizable SBF gradient is observed in NGC 4374, while a small but non-negligible SBF gradient in $V$ and $R$ is observed for NGC 4621, consistent with the known scheme of more metal-poor dominant stellar populations at larger galactocentric radii (e.g., Cantiello et al. 2005). Given that i) $V$ and $R$ are more sensitive to stellar population properties compared to $I$-band SBF (Blakeslee et al. 2001; Cantiello et al. 2003); and ii) $\bar{I}$ gradients up to ~0.4 magnitudes were measured by Cantiello et al. (2005) on similar radial scales for a different set of targets, the negligible $\bar{V}$ and $\bar{R}$ gradients detected here might be explained by the position of the two objects within their host cluster. Since the two targets analysed are located in the regions with highest galaxy density in the Virgo cluster, in fact, this behaviour might be related to the major-merging events in that environment, which tend to smear out possible stellar population gradients (Kobayashi 2004).

Taking advantage of the multi-wavelength coverage of our data set, and of existing $I$, $z$, and $K$-band SBF measurements, we analysed the data of both galaxies in the SBF-colour versus integrated-colour and SBF-colour versus SBF-colour diagrams. This is the first SBF-analysis carried out using SBF data in six different pass-bands. As a result we concluded that the dominant stellar component in the two galaxies is very similar, though NGC 4374 seems to be slightly more metal rich than NGC 4621.

If $B$-band measures are taken into account, the SBF colours of the two galaxies show non-negligible differences, where NGC 4621 has brighter SBF than NGC 4374. Given the known link between SBF magnitudes in blue bands and the properties of a hot old stellar component (Worthey 1993a; Cantiello et al. 2003), we used the SPoT stellar population synthesis code to simulate populations with "non-canonical" properties. In particular, to a solar metallicity old ($t \sim 14$ Gyr) population, we 1) enhanced the content of hot HB stars (i.e., ~50% canonical HB and ~50% HHB); 2) added a very young (down to 30 Myr) diffuse secondary component; and 3) added a more metal-poor SSP (down to [Fe/H] $\sim -2.3$ dex). Within the limits of few data points, and after adopting as a razor the physical plausibility of the population mixing, the simulations seem to favour the HHB component scenario.

This is also supported by Brown et al. (2000, 2008) findings on HHB stars in the compact elliptical galaxy M 32 from UV observations. In this framework, it is relevant to recall that NGC 4621 is substantially brighter than NGC 4374 in the UV bands (Longo et al. 1991) and that the integrated properties of normal elliptical galaxies with bright UV emission are now interpreted as the effect of a diffuse hot stellar component (e.g., Park & Lee 1997). Thus, further analysis is required to better constrain the links between the UV emission and SBF in early type galaxies, also in view of the recent studies on the relation of UV with near-IR SBF amplitudes (Buzzoni & González-López lira 2008). Larger samples of SBF colours in blue bands are required to provide further constraints to this scenario.

Finally, taking the integrated colours and $\bar{V}$ plus $\bar{R}$ SBF into account for the areas of the galaxies where type Ia Supernova exploded, we find no substantial differences between the local and the global stellar population properties in the galaxies. For SN 1939B and its host, NGC 4621, this is also true for $B$-band SBF data. In contrast, there is a $\Delta\bar{B}-\bar{V} \sim 0.4$ mag difference between the regions of the two SNe host in NGC 4374, SN 1957B, and SN 1991bg. Owing the quoted sensitivity of blue-band SBF to stellar population properties, such a difference and, more in general, the scatter in $\bar{B}-\bar{V}$ between the three SNe Ia might be related to different levels of local pollution from a hot stellar component, although for the case of SN 1991bg we cannot exclude the possible systematic effect of a low $\bar{B}$ signal, comparable to the $P_r$ correction.

In conclusion, the present set of SBF measures shows that optical to near-IR SBF magnitudes can be very effective in unveiling the properties of global and/or local stellar populations in distant galaxies. In particular, if $\bar{B}$ (or even SBF in bluer bands) are available, various constraints can be set to show the role of hot field stars in normal ellipticals, at the same time multi-band SBF can be used to analyse the relation between SNe and local stellar population properties. Nevertheless, serious limitations are caused by the small samples of measures still available, making new observations advisable for further study of stellar population properties based on multi-colour SBF analysis.

*Acknowledgements.* M.C. acknowledges the support provided by the PRIN-INAF 2008 (PI. Marconi). We also thank the referee for the very helpful suggestions. Based on data obtained from the ESO Science Archive Facility.

## References

Ajhar, E. A., Tonry, J. L., Blakeslee, J. P., Riess, A. G., & Schmidt, B. P. 2001, ApJ, 559, 584
Barbon, R., Cappellaro, E., & Turatto, M. 1989, A&AS, 81, 421
Bernardi, M., Renzini, A., da Costa, L. N., et al. 1998, ApJ, 508, L143
Bertin, E., & Arnouts, S. 1996, A&AS, 117, 393
Bertola, F. 1964, AJ, 69, 236
Bertola, F., Capaccioli, M., Holm, A. V., & Oke, J. B. 1980, ApJ, 237, L65
Biscardi, I., Raimondo, G., Cantiello, M., & Brocato, E. 2008, ApJ, 678, 168
Blakeslee, J. P., Vazdekis, A., & Ajhar, E. A. 2001, MNRAS, 320, 193
Blakeslee, J. P., Jordán, A., Mei, S., et al. 2009, ApJ, 694, 556
Blakeslee, J. P., Cantiello, M., Mei, S., et al. 2010, ApJ, 724, 657
Brocato, E., Matteucci, F., Mazzitelli, I., & Tornambe, A. 1990, ApJ, 349, 458
Brocato, E., Capaccioli, M., & Condelli, M. 1998, Mem. Soc. Astron. Ital., 69, 155
Brocato, E., Castellani, V., Poli, F. M., & Raimondo, G. 2000, A&AS, 146, 91
Brown, T. M., Bowers, C. W., Kimble, R. A., Sweigart, A. V., & Ferguson, H. C. 2000, ApJ, 532, 308
Brown, T. M., Smith, E., Ferguson, H. C., et al. 2008, ApJ, 682, 319
Buzzoni, A. 1993, A&A, 275, 433
Buzzoni, A., & González-López lira, R. A. 2008, ApJ, 686, 1007
Cantiello, M., Raimondo, G., Brocato, E., & Capaccioli, M. 2003, AJ, 125, 2783
Cantiello, M., Blakeslee, J. P., Raimondo, G., et al. 2005, ApJ, 634, 239
Cantiello, M., Blakeslee, J., Raimondo, G., Brocato, E., & Capaccioli, M. 2007a, ApJ, 668, 130
Cantiello, M., Raimondo, G., Blakeslee, J. P., Brocato, E., & Capaccioli, M. 2007b, ApJ, 662, 940
Cantiello, M., Raimondo, G., Brocato, E., & Biscardi, I. 2009, Mem. Soc. Astron. Ital., 80, 40
Code, A. D., Welch, G. A., & Page, T. L. 1972, in NASA Special Publication, Scientific results from the orbiting astronomical observatory (OAO-2), ed. A. D. Code, 310, 559
Côté, P., Blakeslee, J. P., Ferrarese, L., et al. 2004, ApJS, 153, 223
Folatelli, G., Phillips, M. M., Burns, C. R., et al. 2010, AJ, 139, 120
Freedman, W. L., Madore, B. F., Gibson, B. K., et al. 2001, ApJ, 553, 47
Gallagher, J. S., Garnavich, P. M., Berlind, P., et al. 2005, ApJ, 634, 210
Gallagher, J. S., Garnavich, P. M., Caldwell, N., et al. 2008, ApJ, 685, 752
González, R. A., Liu, M. C., & Bruzual A., G. 2004, ApJ, 611, 270
Hamuy, M., Phillips, M. M., Suntzeff, N. B., et al. 1996, AJ, 112, 2391
Han, Z. 2008, A&A, 484, L31
Howell, D. A. 2001, ApJ, 554, L193
Idiart, T. P., Michard, R., & de Freitas Pacheco, J. A. 2002, A&A, 383, 30
Idiart, T. P., Silk, J., & de Freitas Pacheco, J. A. 2007, MNRAS, 381, 1711
Jensen, J. B., Tonry, J. L., & Luppino, G. A. 1998, ApJ, 505, 111
Jerjen, H., Freeman, K. C., & Binggeli, B. 1998, AJ, 116, 2873
Jerjen, H., Freeman, K. C., & Binggeli, B. 2000, AJ, 119, 166
Jensen, J. B., Tonry, J. L., Thompson, R. I., et al. 2001, ApJ, 550, 503
Jensen, J. B., Tonry, J. L., Barris, B. J., et al. 2003, ApJ, 583, 712
Jerjen, H., Binggeli, B., & Barazza, F. D. 2004, AJ, 127, 771
Jha, S., Riess, A. G., & Kirshner, R. P. 2007, ApJ, 659, 122
Jordán, A. 2004, ApJ, 613, L117
Kaviraj, S., Sohn, S. T., O'Connell, R. W., et al. 2007, MNRAS, 377, 987
Kobayashi, C. 2004, MNRAS, 347, 740
Kosai, H., Kushida, R., Kato, T., Filippenko, A., & Newberg, H. 1991, IAU Circ., 5400, 1
Kuntschner, H., Lucey, J. R., Smith, R. J., Hudson, M. J., & Davies, R. L. 2001, MNRAS, 323, 615
Landolt, A. U. 1992, AJ, 104, 340
Lanoix, P. 1998, A&A, 331, 421
Leibundgut, B., Tammann, G. A., Cadonau, R., & Cerrito, D. 1991, A&AS, 89, 537
Longo, G., Ceriello, A., & Capaccioli, M. 1991, A&AS, 90, 375
Mei, S., Blakeslee, J. P., Côté, P., et al. 2007, ApJ, 655, 144
Minkowski, R. 1964, ARA&A, 2, 247
Pahre, M. A., & Mould, J. R. 1994, ApJ, 433, 567
Park, J., & Lee, Y. 1997, ApJ, 476, 28
Phillips, M. M., Lira, P., Suntzeff, N. B., et al. 1999, AJ, 118, 1766
Press, W. H., Teukolsky, S. A., Vetterling, W. T., & Flannery, B. P. 1992, Numerical recipes in FORTRAN. The art of scientific computing (Cambridge: University Press), 2nd edn.
Raimondo, G. 2009, ApJ, 700, 1247
Raimondo, G., Brocato, E., Cantiello, M., & Capaccioli, M. 2005, AJ, 130, 2625
Riess, A. G., Filippenko, A. V., Challis, P., et al. 1998, AJ, 116, 1009

Schlegel, D. J., Finkbeiner, D. P., & Davis, M. 1998, ApJ, 500, 525
Scott, N., Cappellari, M., Davies, R. L., et al. 2009, MNRAS, 398, 1835
Sersic, J. L. 1968, Atlas de galaxias australes (Cordoba, Argentina: Observatorio Astronomico)
Shopbell, P. L., Bland-Hawthorn, J., & Malin, D. F. 1993, AJ, 106, 1344
Sirianni, M., Jee, M. J., Benítez, N., et al. 2005, PASP, 117, 1049
Sodemann, M., & Thomsen, B. 1996, AJ, 111, 208
Tonry, J., & Schneider, D. P. 1988, AJ, 96, 807
Tonry, J. L., Ajhar, E. A., & Luppino, G. A. 1990, AJ, 100,1416
Tonry, J. L., Blakeslee, J. P., Ajhar, E. A., & Dressler, A. 2000, ApJ, 530, 625
Tonry, J. L., Dressler, A., Blakeslee, J. P., et al. 2001, ApJ, 546, 681
Turatto, M., Benetti, S., Cappellaro, E., et al. 1996, MNRAS, 283, 1
Wang, X., Wang, L., Pain, R., Zhou, X., & Li, Z. 2006, ApJ, 645, 488
Worthey, G. 1993a, ApJ, 415, L91
Worthey, G. 1993b, ApJ, 409, 530
Worthey, G. 1994, ApJS, 95, 107
Zwicky, F. 1942, ApJ, 96, 28